Babol University Of Medical Sciences

IJMCM, Summer 2025, VOL 14, NO 3

International Journal of Molecular and Cellular Medicine

Journal homepage: www.ijmcmed.org

ORIGINAL ARTICLE

Potential Protective Effects of Cerium Oxide Nanoparticles on Ultraviolet-B Irradiated Fibroblast Cells

Reza Fardid[1], Mansooreh Mostafavi Mendi[1*], Gholamhassan Haddadi[1], Mohammad Ali Takhshid[2]

1. Department of Radiology, School of Paramedical Sciences, Shiraz University of Medical Sciences, Shiraz, Iran.
2. Department of Laboratory Sciences, School of Paramedical Sciences, Shiraz University of Medical Sciences, Shiraz, Iran.

ARTICLE INFO

Received: 2024/12/18
Revised: 2025/05/24
Accepted: 2025/06/9

ABSTRACT

Increased environmental ultraviolet-B (UVB) exposure stimulates reactive oxygen species (ROS) overproduction, disrupts cellular redox balance, and contributes to skin disorders. Antioxidants inhibit autoxidation by neutralizing or suppressing free radicals. Certain nanomaterials, like cerium oxide nanoparticles (CNPs), function as antioxidants under specific conditions. Through their redox and catalytic properties, CNPs scavenge ROS, mitigate oxidative damage, and may help prevent skin injuries. While most research targets ionizing radiation, studies exploring CNPs under non-ionizing UVB remain limited. To address this, the study evaluates their photochemoprotective effects in UVB-exposed L929 fibroblasts. The 3-(4, 5-dimethylthiazol-2-yl)-2, 5-diphenyltetrazolium bromide (MTT), cupric ion reducing antioxidant capacity (CUPRAC), dichloro-dihydro-fluorescein diacetate (DCFH-DA), and annexin V/propidium iodide (annexin V/PI) assays were used to evaluate cell viability, oxidative stress, and apoptosis. Cell viability was assessed using the MTT assay at CNP concentrations of 10, 50, and 100 µM and UVB intensities of 150–900 mJ/cm², selected based on prior physiologically relevant in vitro studies. At 600 mJ/cm² UVB, cell viability decreased by 45% (MTT assay). Treatment with 50 µM CNP significantly increased total antioxidant capacity relative to untreated controls (CUPRAC assay, $p = 0.0018$). CNP and UVB effects on ROS production and apoptosis were evaluated separately and in combination using DCFH-DA and annexin V/PI assays. Results show that pretreatment with CNPs before UVB radiation impedes cell apoptosis and reduces ROS, suggesting that CNPs mitigate UVB-induced oxidative damage in L929 cells by restoring oxidative balance through their redox activity and ROS-scavenging properties. These findings indicate CNP-based interventions may offer therapeutic strategies against UVB-induced skin and related disorders.

Keywords: Antioxidant, Cerium oxide nanoparticles, L929 fibroblasts, Reactive oxygen species, UVB-induced damage

***Corresponding**:
Mansooreh Mostafavi Mendi
Address:
Department of Radiology, School of Paramedical Sciences, Shiraz University of Medical Sciences, Shiraz, Iran
E-mail:
mostafavimm3@mums.ac.ir, surehmendi@gmail.com

Cite this article: Fardid R, et al. Potential Protective Effects of Cerium Oxide Nanoparticles on Ultraviolet-B Irradiated Fibroblast Cells. International Journal of Molecular and Cellular Medicine. 2025; 14 (3):0 - 0. DOI: 0

Introduction

Overexposure to ultraviolet radiation (UVR), from both natural sunlight and artificial sources such as lasers and fluorescent lamps, along with the thinning of the ozonosphere, contributes to adverse health outcomes. The skin, as the largest bodily organ, is particularly susceptible to diseases such as sunburn, skin aging, inflammation, and cancer (1). To better understand the risks of solar radiation on cellular health and identify effective protective strategies, further investigation into ultraviolet (UV) components is necessary.

UVR, a non-ionizing form of radiation in the electromagnetic wave range, comprises three distinct parts: ultraviolet-A (UVA: 315-400 nm), ultraviolet-B (UVB: 280-315 nm), and ultraviolet-C (UVC: 100-280 nm). The proportion of ultraviolet radiation containing UVA and UVB waves that makes it to the Earth's surface is roughly five percent. UVC rays are mainly absorbed by the ozonosphere, while a significant proportion of UVA (about 90 to 95%) and a smaller percentage of UVB (about 5 to 10%) radiation reach the Earth's surface (2). Therefore, most UV-related health damage on earth is attributed to UVA and UVB rays (3). UVR stimulates intracellular chromophores that generate reactive oxygen species (ROS). Given their essential role in protective cellular functions and physiological processes, ROS at moderate concentrations are necessary for human health (4).

ROS include various molecules, and in certain microenvironmental contexts, these diverse species may interact with other biomacromolecules such as deoxyribonucleic acid (DNA), proteins, and lipids, thereby contributing to oxidative stress (5). While both radical and non-radical ROS, such as hydroxyl radical ($OH^{\bullet}$), hydrogen peroxide (H_2O_2), and superoxide anion ($O_2^{\bullet -}$), are involved in provoking cellular changes such as UV-induced oxidative stress, $OH^{\bullet}$ has significant oxidization properties in comparison to the weak reactivity of H_2O_2 and $O_2^{\bullet -}$ (6, 7). Prolonged ROS exposure accelerates aging and contributes to various diseases (8). Unrepaired UV-damaged cells may either undergo apoptotic cell death due to loss of viability or survive with genetic changes that lead to cancer (9).

UVR induces significant cellular oxidative stress, particularly through UVA (10). Studies have shown that human skin molecules, such as endogenous photosensitizers or chromophores, absorb UV energy upon UVA exposure and interaction, then transfer it to other molecules, including oxygen, ultimately leading to ROS production (11, 12). Such ROS can inflict oxidative damage and impair the antioxidant defense system, disturbing the delicate balance required for cellular homeostasis. When this balance is disrupted, oxidative stress ensues, potentially leading to apoptosis or even carcinogenesis (13).

Although oxidative damage is a key concern, the precise molecular mechanisms underlying UVA mutagenesis and subsequent DNA damage responses triggered by UVA and UVB interaction, as well as their mutagenic consequences, remain subjects of ongoing research (14). Generally, depending on environmental and individual factors, UVB radiation may cause photochemical damage after reaching susceptible cellular regions (15). The complementary effects of UVA and UVB have prompted the development of photoprotective strategies, including filters and UV-absorbing materials with antioxidant capabilities aimed at mitigating skin damage, while also encouraging further investigation into their broader cellular impacts, particularly those involving cell death and stress responses.

In particular, UVB rays, which penetrate the full thickness of the epidermis and the uppermost layer of the dermis, can trigger ROS production, potentially harming both epidermal keratinocytes and dermal fibroblasts (16). Despite the skin's intrinsic antioxidant defense mechanisms, prolonged and frequent UV radiation can impair this system and provoke a cascade of biochemical changes (17, 18). These alterations can lead to cell death via necrosis or apoptosis (19). In the case of apoptosis, UVB-irradiated cells initiate this process by activating apoptotic mediators such as caspase and Bax (20).

On the nanoscale, cerium (Ce), the most reactive chemical element among rare-earth metals, has several applications, including UV absorbers, oxygen sensors, catalysts, and fuel additives. (21-25). These properties have also led to increasing interest in nanomedicine applications. Cerium oxide nanoparticles (CNPs), owing to their ability to toggle between Ce^{3+} and Ce^{4+} oxidation states, mimic the catalytic activity of key antioxidant enzymes such as catalase and superoxide dismutase (SOD) through a redox cycling mechanism (26, 27). This redox cycling occurs through the sequential oxidation and reduction of Ce atoms on

the nanoparticle surface: Ce^{4+} accepts an electron, reducing to Ce^{3+} and releasing molecular oxygen (O_2); Ce^{3+} then donates an electron to a second $O_2^{\bullet-}$, regenerating Ce^{4+} and forming H_2O_2. This reversible process allows CNPs to continuously scavenge reactive oxygen species without being consumed or undergoing nanoparticle degradation. Importantly, surface oxygen vacancies, which are more prevalent in smaller or defect-rich particles, stabilize the Ce^{3+} state and enhance redox efficiency (28, 29). This regenerative surface chemistry of CNPs underlies their sustained antioxidant function, enabling them to actively react with low-reactive ROS such as H_2O_2 and $O_2^{\bullet-}$, as well as reactive nitrogen species (RNS), in cellular and animal models, thereby preventing ROS accumulation and ultimately enhancing cell viability (30).

More research has focused on the application of CNPs for oxidative stress-related disorders as a result of their antioxidant qualities. Despite extensive interest in CNPs' biomedical potential, the mechanistic underpinnings of this enzyme-like activity, particularly how redox cycling is modulated by physicochemical factors such as oxygen vacancy density, remain underexplored. Addressing this gap is essential to optimizing CNPs for therapeutic use in oxidative stress–related diseases (29). In this context, efficient methods to avoid skin injuries provoked by UVR involve hindering ROS formation and enhancing ROS scavenging. In another study, it has been shown that CNPs, by reducing ROS levels and raising antioxidant enzyme activities, control oxidative damage caused by UVB in fibroblast cells (31). Other studies on oxidative stress situations and CNP interactions in such contexts specify changes in transcription levels of glutathione and superoxide dismutase 2, mitochondrial (SOD_2, also known as manganese-dependent superoxide dismutase). Accordingly, CNP pre-incubation (i.e., before irradiation) effects and distinguishable sustained antioxidant activities are validated by such gene expression alternations (32-34).

While the carcinogenic effects of UV radiation are well-documented, the detailed molecular mechanisms of UVB-induced oxidative damage and the specific interactions of antioxidants like CNPs with skin cells remain insufficiently explored. Understanding how CNPs interact with the cellular microenvironment under oxidative stress conditions is essential for developing targeted protective strategies. This study addresses that gap by investigating the effects of CNP pretreatment on ROS production, cell viability, and apoptosis in UVB-irradiated L929 fibroblasts. CNP pretreatment is hypothesized to mitigate UVB-induced cellular damage by reducing ROS levels, enhancing antioxidant defenses, and preserving cell viability in L929 fibroblasts. To evaluate this hypothesis, the relationships among cell viability, ROS production, and antioxidant capacity induced by CNPs under UVB exposure are assessed, focusing on their combined role in mitigating UVB-induced cellular damage.

Methods

Chemicals

Fetal bovine serum (FBS), trypsin-EDTA (0.25%), and phosphate-buffered saline (PBS) tablets were obtained from Gibco (Thermo Fisher Scientific, Waltham, MA, USA). Dimethyl sulfoxide (DMSO), trypan blue dye, and Giemsa stain for microscopy were obtained from Merck (Merck KGaA, Darmstadt, Germany). Also, thiazolyl blue tetrazolium bromide known typically as MTT (methylthiazolyldiphenyl-tetrazolium bromide) powder, was purchased from Sigma-Aldrich (Merck KGaA, Darmstadt, Germany). Roswell Park Memorial Institute 1640 (RPMI 1640) medium, penicillin, and streptomycin were purchased from Shellmax (Zhejiang, China). Cerium oxide nanoparticles (CNP nanopowder, CeO_2, 99.97%, 10-30 nm) were obtained from US Research Nanomaterials, Inc. (Houston, TX, USA). The Fluorescein Isothiocyanate (FITC) apoptosis detection kit I was purchased from BD Pharmingen™ (BD Biosciences, San Jose, CA, USA). The reactive oxygen species detection assay kit was bought from Teb Pazhouhan Razi (TPR Innovative, Tehran, Iran). The total antioxidant capacity (TAC) assay kit was purchased from Kiazist Pishro Barman (Hamedan, Iran). All other chemicals used were of analytical grade and commercially available.

Cell Culture

L929 fibroblast cells (subcutaneous connective mouse tissue), purchased from Pasteur Institute (Tehran, Iran), were cultured in RPMI 1640, 10% FBS, and 1% penicillin-streptomycin in humidified surroundings with 5% carbon dioxide (CO_2) under 37 $^{\circ}$C temperature conditions. The cells were used up to passage twenty. The L929 cell line was used to

investigate toxicity, including phototoxicity, as an in vitro test system. Prior research has pointed out L929 fibroblast cells' photosensitivity toward UV radiation (35), a characteristic that has made them a widely accepted in vitro model for studying UV-induced oxidative stress and evaluating the photoprotective effects of therapeutic compounds.

CNP Characterization

CNP contained ten grams of 99.97% CNP powder with sizes ranging from 10 to 30 nm. Transmission electron microscopy (TEM) was used to scrutinize the grain size and morphology of CNP.

CNP Suspension Preparation

To prepare a 0.027 M stock solution of CNPs, 9.3 mg of CNP powder was weighed and suspended in 2 mL of serum-free RPMI 1640 medium. The molecular weight (MW) of cerium oxide (CeO_2) was taken as 172.115 g/mol, assuming pure CeO_2 composition. The required mass of CNP powder was calculated using the formula for molarity (M):

mass (g) = M × MW (g/mol) × volume (L)

Substituting the values:

0.027 mol/L × 172.115 g/mol × 0.002 L = 0.0093 g

The suspension was vortexed thoroughly and stored at 4 ˚C. Working dilutions were freshly prepared before each experiment using complete RPMI 1640 medium.

UVB Irradiation

A Philips broadband lamp with a wavelength of 290 to 315 nm, 19.3 watts power, and a voltage of 59 volts that emitted UVB spectrum (UVB Broadband TL 20W/12 RS SLV/25, Germany) was used for irradiation. This lamp is suitable for various applications such as phototherapy, agriculture, and therapy. For irradiation purposes, the cell culture plate was placed at a distance of 20 cm from the lamp. Also, for measuring the intensity of radiation, a UVB spectrum-sensitive UV-meter (UV-340A Lutron) placed at a distance of 20 cm from the lamp was used. Various UVB radiation intensities (150-900 mJ/cm^2) were set up for cell exposure. Eventually, the irradiation intensity that led to around 45% reduction in non-treated L929 fibroblasts' viability was chosen to assess the protective potential of CNPs.

Cell Viability Assay

The effect of CNP on the viability of L929 fibroblast cells was evaluated by utilizing the MTT assay as a cytotoxic assay, as originally described by Mosmann (36). The MTT test is a colorimetric method that performs the final analysis based on the reduction and breaking of yellow tetrazolium crystals by dehydrogenated succinate enzyme and the formation of insoluble purple crystals (37, 38).

The final concentration of 5×10^3 cells/well was selected for cell seeding in a volume of 200 µL in 96-well plates. After 24 hours of incubation, the cells were treated with various concentrations of CNP (10, 50, and 100 µM) for an additional 24 hours. Following treatment, the supernatant was removed from each well under dark conditions, and 20 µL of MTT solution (5 mg/mL) was added. The plate was then covered with aluminum foil. The plate was incubated for 4 hours at 37 ˚C. After incubation, the MTT solution was removed, and 100 µL of DMSO was added to each well to dissolve the formazan crystals. The plate, covered with aluminum foil, was shaken for 15 minutes to allow complete formazan solubilization and color development. Absorbance was then measured at 570 nm (reference 630 nm) using a microplate reader (Stat Fax-2100).

For UVB-irradiated cells, following the 24-hour CNP treatment, the cells were directly exposed to UVB light for 40 minutes (600 mJ/cm²). The MTT assay was then performed following the same procedure previously described for non-irradiated cells.

Quantification of Total Antioxidant Capacity

The total antioxidant capacity of the samples was assessed using the CUPRAC (cupric ion reducing antioxidant capacity) assay, as described by Özyürek et al. (39). In this method, cupric ions (Cu^{2+}) are reduced to cuprous ions (Cu^{+}) in the presence of antioxidants, forming a yellow-orange chromogen that is absorbent at 450 nm.

The assay utilized a calibration curve generated with Trolox at concentrations of 0-400 nmol/mL, as detailed in Figure 3A, with the derived equation y = 0.0009x + 0.0188. Sample antioxidant capacities were calculated based on this calibration curve. The total antioxidant capacity was normalized to cell number to account for any differences in cell count between the control and treated groups.A total of 4×10^5 cells were seeded in 6-well plates with a final volume of 2 mL per well. After 24 hours of incubation, cells were treated

with 50 µM CNP for an additional 24 hours. Following treatment, the supernatant was removed and the cells were trypsinized. After centrifugation, the supernatant was discarded. For cell lysis, the pellet was resuspended in PBS and subjected to three freeze-thaw cycles. Then, 30 µL of each sample or standard was added to the wells of a microplate. PBS was used as the blank, with 30 µL added to designated blank wells. Subsequently, 150 µL of TAC working solution was added to each well. Plates were incubated at room temperature for 30–60 minutes. Finally, absorbance was measured at 450 nm.

Evaluation of Intracellular ROS Production

The fluorescent probe DCFH-DA (2′,7′-dichlorodihydrofluorescein diacetate) was used for ROS detection following Eruslanov and Kusmarts' (40) explanations, despite doubts about its limitations in terms of specificity (41, 42). Intracellular ROS scavenging capacity was determined using the fluorescent ROS probe DCFH-DA, which is transformed into a non-fluorescent compound, DCFH (2′,7′-dichlorodihydrofluorescein), via esterase after entering the cell. The compound is then immediately oxidized to DCF (2′,7′-dichlorofluorescein) in the presence of ROS and emits a fluorescent compound. The intensity of the emitted fluorescence is related to the level of intracellular ROS (43).

A 6-well plate was used to culture 4×10^5 cells in a final volume of 2 mL. 24 hours after seeding, cell treatment was performed with the 50 µM CNP concentration for 24 hours, after which cells were exposed to UVB for forty minutes (600 mJ/cm^2). Next, the cells were detached and incubated with 100 µL of the prepared DCF dye for one hour at 37 ˚C in the dark. The reading was conducted by flow cytometry (BD FACSCalibur).

Evaluation of Apoptosis Rate

For the measurement of the apoptotic cells, an FITC Apoptosis Detection Kit I was used. Cell cultivation was performed in 6- well plates at a density of 4×10^5 per well and incubated for 24 hours. Next, 50 µM of CNP was added to cells for 24 hours, and eventually, they were exposed to 600 mJ/cm^2 of UVB. After irradiation, the cells were detached and washed with 1X Binding Buffer. The cells were mixed with 5 µL of PI dye and 5 µL of FITC Annexin V and incubated for 15 minutes in the dark. Finally, the cell precipitate was dissolved in 150 µL of 1X Binding Buffer solution. The reading and analysis were performed using flow cytometry.

Statistical Analysis

All experiments were performed in triplicate (technical replicates), and the results presented are from a single representative experiment. Although the experiment was repeated independently for procedural familiarization, those additional runs were not included in the final statistical analysis. Statistical significance was determined by one-way analysis of variance (ANOVA) followed by Tukey's post hoc test, with $p < 0.05$ considered significant. Data are expressed as mean ± standard deviation (SD). FlowJo, GraphPad Prism 8, and Excel software were used for data analysis.

Results

Particle Size and Morphology of CNP

The grain size of CNP averages 30 nm, and the shape of the nanoparticles is spherical, as seen in the TEM image (Figure 1).

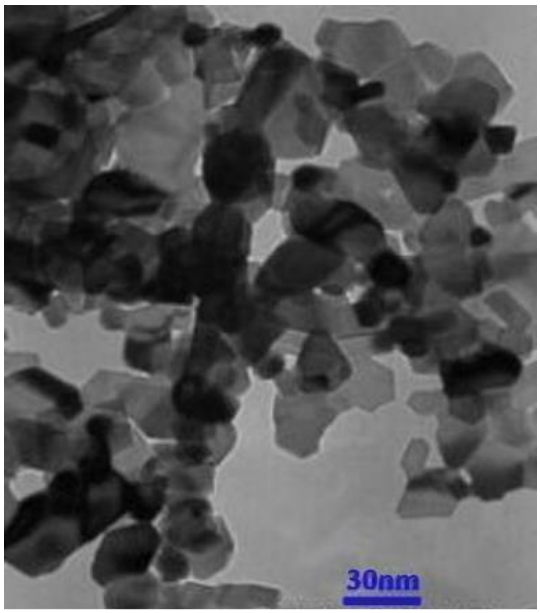

Figure 1. Particle size and morphology of CNP. TEM images of CNP indicate a spherical shape with an approximate diameter of 30 nm in size.

Non-Toxic CNP and its Protective Effects against UVB Radiation

The MTT assay results of this study indicated that concentrations of 10, 50, and 100 µM of CNP did not

demonstrate a significant difference compared to the control group in cell viability 24 hours after treatment (Fig. 2A). In Fig. 2B, the outcome of different intensities of UVB radiation on cell viability is shown. According to the results, cell viability was reduced as a result of UVB radiation in a dose- and time-dependent manner. In comparison to the control group (without radiation and treatment), radiation with intensities of 450, 600, 750, and 900 mJ/cm^2 had a remarkable reduction in the percentage of cell viability, whereas intensities of 150 and 300 mJ/cm^2 led to a minor decrease in cell viability. Regarding the results, the intensity chosen to assess the protective ability of the CNP against UVB radiation was 600 mJ/cm^2 (40 minutes), which led to a decline of around 45% in the viability of non-treated L929 fibroblast cells.

CNP was found to be non-cytotoxic to L929 fibroblast cells. Therefore, the effect of CNP against UVB radiation was initially assessed by the CNP treatment and then irradiation using an MTT assay. Fig. 2C shows a significant decrease in cell viability in the UVB-irradiated group compared to the control group. Concentrations of 10, 50, and 100 µM of CNP before irradiation led to a significant increase in cell viability compared to the UVB-irradiated group. For further experimental observations, ultimately, 50 µM of CNP for treatment before irradiation was selected since this concentration increased cell viability as compared to the UVB-irradiated group to a greater extent than other concentrations (Figure 2).

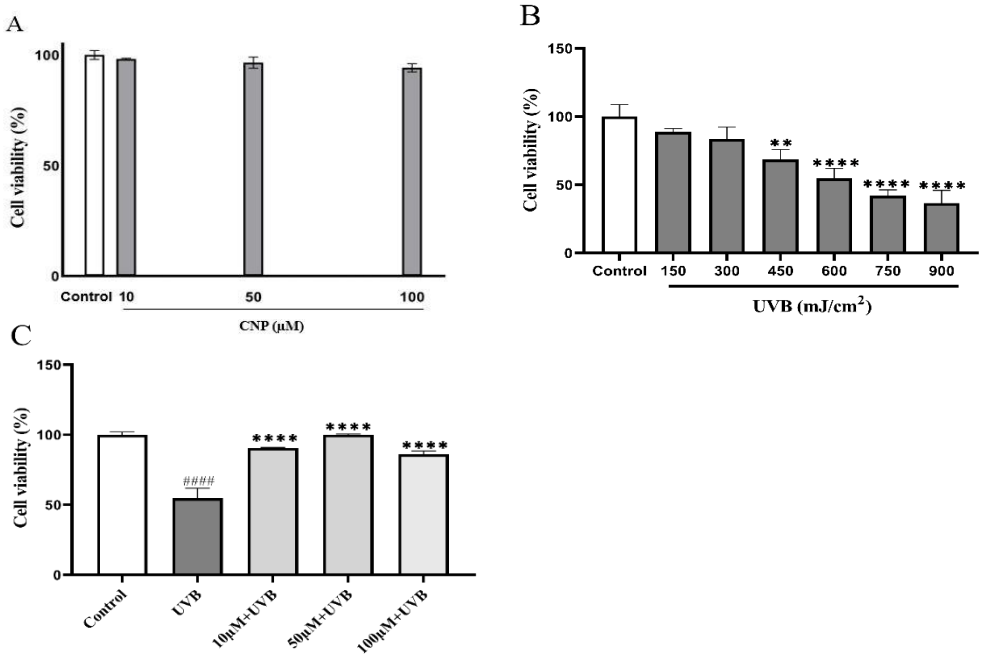

Figure 2. CNP concentrations of 10, 50, and 100 µM display non-toxicity for L929 fibroblasts with significant increases in cell viability compared to the UVB irradiated group. (A) L929 fibroblasts were treated with different concentrations (10, 50, and 100 µM) of CNP. (B) L929 fibroblasts were irradiated at different intensities of UVB radiation (150-900 mJ/cm2). (C) L929 fibroblasts were treated with 10, 50, and 100 µM CNP for 24 hours before irradiation with 600 mJ/cm2 UVB. (Control) cells non-treated and non-irradiated, (UVB) cells irradiated with 600 mJ/cm2 UVB and non-treated, (10 µM + UVB) cells treated with 10 µM of CNP and irradiated, (50 µM + UVB) cells treated with 50 µM of CNP and irradiated, (100 µM + UVB) cells treated with 100 µM of CNP and irradiated. The results are expressed as a percentage of control. Each column represents the mean ± SD (n = 3). (B): **p = 0.0017, ****p < 0.0001 significant difference compared with ontrol. (C): ####p < 0.0001 significant difference compared with Control. ****p < 0.0001 significant difference compared with UVB.

CNP Leads to an Increase in Total Antioxidant Capacity in L929 Fibroblasts

To evaluate the total antioxidant capacity of cells treated with CNP and the control group, it is first

necessary to draw a standard curve. According to Fig. 3A, a standard curve was plotted at Trolox concentrations of 0, 40, 80, 160, 200, and 400 nmol/mL at an absorption wavelength of 450 nm. Finally, by calculating the optical density (OD) of the control and CNP groups, the total antioxidant capacity can be calculated using the standard Trolox curve. Regarding this curve and the equation that defines it (y = 0.0009x + 0.0188), the antioxidant concentration of the control group is 34.66 ± 1.57 nmol/mL, and the treated group with a concentration of 50 µM is 118 ± 4.716 nmol/mL. The antioxidant capacity was normalized to cell number. Fig. 3B illustrates that the total antioxidant capacity significantly increased in cells treated with 50 µM of CNP in comparison to the control group (Figure 3).

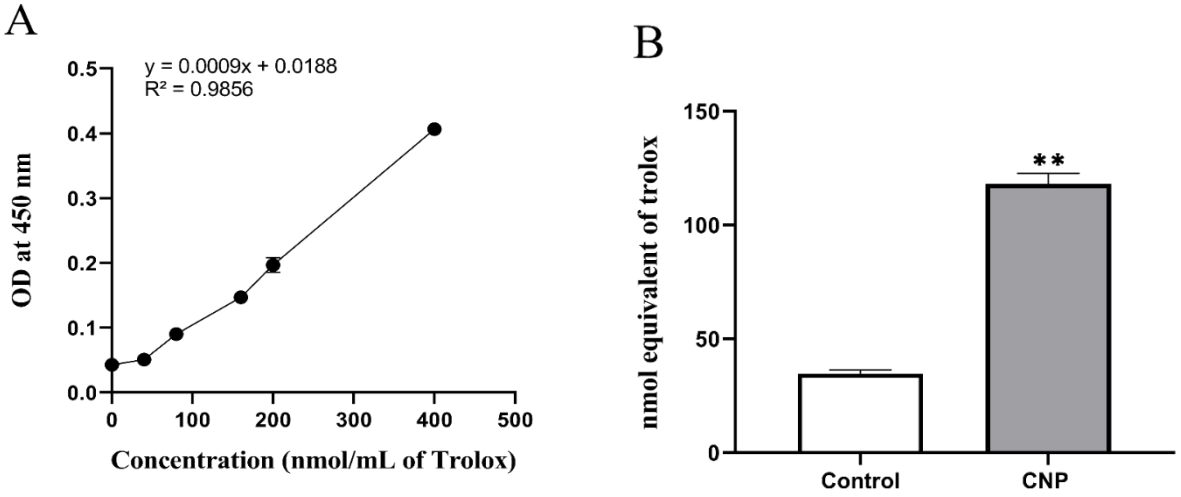

Figure 3. CNP leads to an increase in total antioxidant capacity in L929 fibroblasts compared to the control group. (Control) cells non-treated and non-irradiated, (CNP) cells treated with 50 µM of CNP. (A) Standard curve was plotted at Trolox concentrations of 0, 40, 80, 160, 200, and 400 nmol/mL at the absorption wavelength of 450 nm, (B) CNP leads to a significant increase in total antioxidant capacity in L929 fibroblasts compared to the control group. According to the standard curve line equation of Trolox (y = 0.0009x + 0.0188, R2 = 0.985) the antioxidant concentration of the control group is 34.66 ± 1.57 nmol/mL and the treated group with a concentration of 50 µM is 118 ± 4.716 nmol/mL. **p = 0.0018 significant difference compared with Control.

Reduction of ROS Formation by CNP in UVB-Irradiated L929 Cells

As shown in Fig. 4A and B, UVB irradiation at 600 mJ/cm² significantly increased intracellular ROS levels in L929 fibroblasts, with a geometric mean fluorescence intensity of 1.303 ± 0.4186, compared to the control group. Pretreatment with 50 µM CNP for 24 hours prior to UVB exposure resulted in a marked reduction in ROS levels, with a geometric mean of 0.2767 ± 0.01155, compared to the UVB-only group. These results demonstrate that CNP significantly attenuates ROS production in UVB-irradiated L929 fibroblast cells (p = 0.003) (Figure 4).

CNP Decreases Apoptosis Production in UVB-Irradiated L929 Cells

The annexin V/propidium iodide (annexin V/PI) assay was used to evaluate the effect of CNP on the reduction of apoptotic cell ratio in UVB-irradiated cells. Fig. 5A presents strip plots of L929 cells with annexin V/PI staining. The coordinate axis (FL1-H) illustrates the fluorescence logarithm of annexin V conjugated with fluorescein isothiocyanate (Annexin V-FITC), and the coordinate axis (FL2-H) represents the fluorescence intensity of propidium iodide (PI). FITC is excited by blue light at a wavelength of 493 nm and emits green fluorescence at a wavelength of 525 nm. PI is excited by green-blue light at 540 nm and emits red fluorescence at 620 nm. As shown in Fig. 5B, total apoptosis (sum of early and late apoptosis) was significantly higher in the UVB group compared to the control (P = 0.0018), while pretreatment with CNP

(CNP+UVB) significantly reduced apoptotic cell percentage compared to UVB alone (P = 0.0079).

Fig. 5C shows that necrosis slightly increased in the UVB group compared to the control, although this difference was not statistically significant. Necrosis was marginally reduced in the CNP+UVB group relative to UVB. However, CNP treatment alone significantly increased necrosis compared to the UVB, CNP+UVB, and control groups (P = 0.0332, P = 0.0245, P = 0.0099, respectively). According to Fig. 5D, late apoptosis significantly increased in the UVB group compared to the control group (P = 0.0007) and significantly decreased in the CNP+UVB group relative to the UVB group (P = 0.0043). Fig. 5E indicates that early apoptosis showed a non-significant increase in the UVB group compared to the control and a non-significant decrease in the CNP+UVB group compared to the UVB group. Fig. 5F shows that the proportion of live cells significantly decreased in the UVB group compared to the control (P = 0.0062) and significantly increased in the CNP+UVB group relative to the UVB group (P = 0.0339). Notably, live cell percentage significantly reduced in the CNP group compared to the control group (P = 0.0238) (Figure. 5).

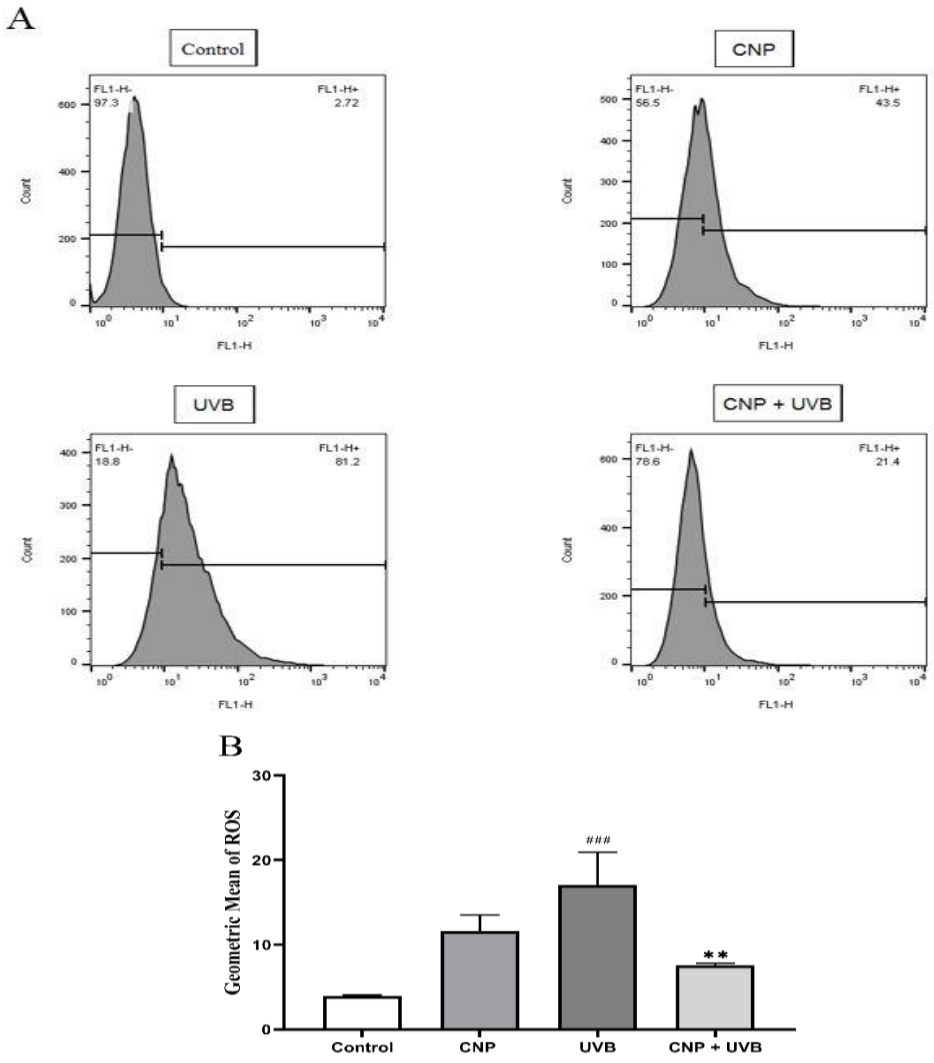

Figure 4. Reduction in ROS produced in L929 cells pretreated with 50 µM CNP concentrations and irradiated with UVB in comparison to the UVB irradiated group. Intracellular ROS were measured by flow cytometry using an oxidation-sensitive fluorescent probe, DCFH-DA which is oxidized to DCF in the presence of ROS. (Control) cells non-treated and non-irradiated, (UVB) cells irradiated with 600 mJ/cm^2 UVB and non-treated, (CNP + UVB) cells treated for 24 hours with 50 µM CNP and irradiated, (CNP) cells treated for 24 hours with 50 µM CNP. (A) The intracellular ROS histogram is presented for all groups. FL1-H$^+$ indicates positive intracellular ROS. FL1-H$^-$ indicates negative intracellular ROS. Guidelines have been drawn through histograms for means of comparison. (B) Quantification of the fluorescence intensities of the images in panel

(A). The geometric mean indicates the intensity of fluorescence emitted from cells containing ROS, which is a more accurate criterion for reporting. Each column represents the mean ± SD (n = 3). ###p = 0.0003 significant difference compared with Control. **p = 0.003 significant difference compared with UVB.

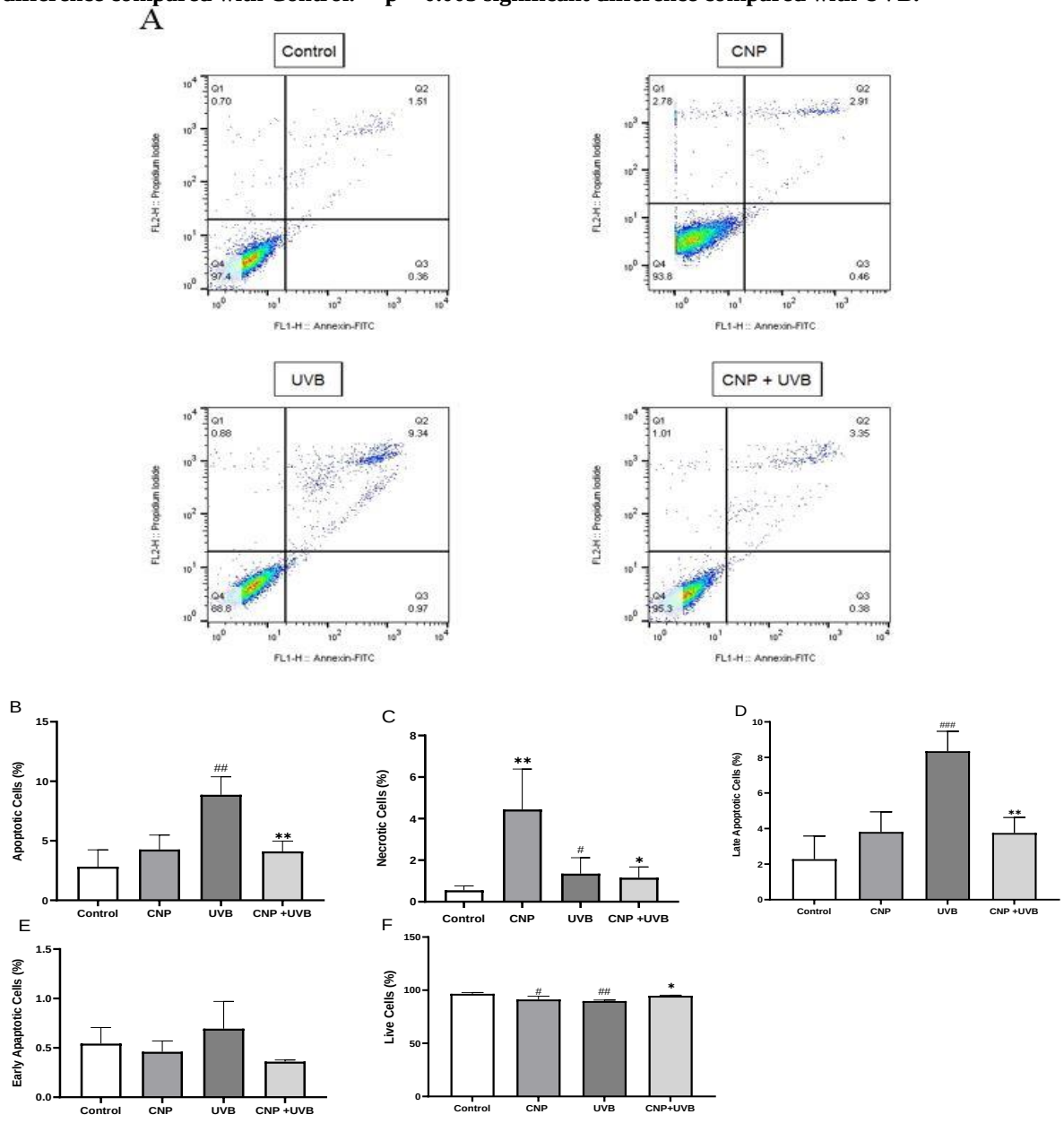

Figure 5. Reduction in generated apoptosis in L929 cells pretreated with 50 µM CNP concentrations and irradiated with UVB in comparison to the UVB irradiated group. Percentage of the apoptotic L929 cells pretreated with CNP and irradiated with UVB measured by flow cytometry using Annexin V- FITC and PI double staining. (Control) cells non-treated and non-irradiated, (UVB) cells irradiated with 600 mJ/cm^2 UVB and non-treated, (CNP + UVB) cells treated for 24 hours with 50 µM CNP and irradiated, (CNP) cells treated for 24 hours with 50 µM CNP. (A) Representative dot plots of annexin V/PI staining of L929 cells (bottom left quadrant (Q4): viable cells, bottom right quadrant (Q3): cells undergoing apoptosis, top right quadrant (Q2): dead cells in the late stage of apoptosis, top left quadrant (Q1): Necrotic cells). (B) General Apoptosis, ##p = 0.0018 significant difference compared with Control. **p = 0.0079 significant difference compared with UVB. (C) Necrotic cells, **p = 0.0099 significant difference compared with Control. #p = 0.0332 significant difference compared with CNP. *p = 0.0245 significant difference compared with CNP. (D) Late apoptotic cells, ###p = 0.0007 significant difference compared with Control. **p = 0.0043 significant difference compared with UVB.

(E) Early apoptotic cells. (F) Live cells, #p = 0.0238 significant difference compared with Control, ##p = 0.0062 significant difference compared with Control, *p = 0.0339 significant difference compared with UVB. Each column represents the mean ± SD (n = 3).

Discussion

This study demonstrated that CNPs exert a protective effect against UVB-induced oxidative damage in L929 fibroblast cells. The MTT assay indicated that concentrations of 10, 50, and 100 μM of CNP, 24 hours after treatment, did not cause a significant difference in cell viability compared to the control group, suggesting that low concentrations of CNP are not cytotoxic to L929 fibroblasts. The CUPRAC method confirmed that CNPs impeded UVB-induced oxidative processes, exhibiting antioxidant-like behavior at the chemical level. This effect was further validated at the cellular level by the DCFH-DA assay, which demonstrated that CNPs attenuated intracellular ROS levels in UVB-irradiated L929 fibroblast cells. Given that elevated ROS levels directly contribute to apoptosis, flow cytometric analysis confirmed that CNP pretreatment significantly reduced UVB-induced apoptosis in the L929 cell line. This protective effect aligns with the observed ability of CNPs to suppress ROS accumulation induced by UVB exposure.

Although the present findings indicate no cytotoxicity associated with CNP treatment, UVB exposure alone contributes to substantial cell death in L929 fibroblasts by impairing mitochondrial dehydrogenase activity and compromising membrane integrity (44). These results align with prior studies reporting the cytoprotective effects of CNPs against various toxicities (45-47). With the exception of the 5 μM concentration, which was not tested in the current study, the findings corroborate earlier work reporting no significant difference in L929 cell viability compared to the control group following 24-hour exposure to CNP concentrations of 5, 10, 50, and 100 μM (31). However, a slight variation was noted: whereas the earlier study reported a non-significant increase in viability, the current data showed a non-significant decrease. This variation may result from differences in nanoparticle synthesis methods and physicochemical properties, as the previous study used wet-chemistry-synthesized particles measuring 3–5 nm, and smaller nanoparticles are generally more toxic due to their larger surface area-to-volume ratio (48). Additionally, differences in cellular physiology, including antioxidant responses, or variations in culture media conditions may also influence cytotoxicity outcomes, as supported by studies on oxidative stress induced by cerium oxide nanoparticles in cultured BEAS-2B cells (49). Consistent with this, another study that treated L929 cells with nanoceria concentrations of 5, 10, 50, 100, 250, and 500 nM, using particles within the 3 to 5 nm range, similarly reported no impact on viability after 24 hours, thereby further supporting the findings of the present study (45). After it was found that CNPs were nontoxic to L929 cells in the present study, their protective potential against UVB-induced cytotoxicity was evaluated. L929 cells were exposed to various concentrations of CNP in combination with UVB radiation (600 mJ/cm²) delivered from a distance of 20 cm. As hypothesized, UVB exposure alone resulted in a significant reduction in cell viability compared to the control group ($P < 0.0001$). In contrast, co-treatment with 50 μM CNP significantly improved cell viability relative to the UVB-only group ($P < 0.0001$), indicating a cytoprotective effect. Accordingly, 50 μM was selected as the protective concentration for further experiments.

In the earlier study that reported no significant change in L929 cell viability after 24-hour exposure to CNP concentrations of 5, 10, 50, and 100 μM, the 10 μM concentration was used as a protective dose, applied 24 hours before UVB irradiation at 500 mJ/cm² from a distance of 20 cm (31). The difference in protective concentration observed between that study and the present one may be attributed to the lower UVB intensity used in that setup, along with the specific nanoparticle characteristics already discussed.

Fibroblast cells play a central role in maintaining skin integrity by synthesizing extracellular matrix components, such as collagen, which support skin elasticity and firmness. Previous studies have demonstrated that fibroblast cell lines are susceptible to photodamage and photoaging following UVB irradiation (31, 35, 50-55). Ultraviolet light is known to be harmful to fibroblast cells, leading to the inhibition of pro-collagen synthesis and the degradation of dermal fibers, both of which are key contributors to photoaging (56). Given these findings, preserving fibroblast cells and protecting them from

photo-induced damage is essential. This study aimed to elucidate the cytoprotective and antioxidant mechanisms of CNPs in mitigating UVB-induced oxidative stress and apoptosis in L929 fibroblast cells.

To contextualize these results, the UVB intensities (150–900 mJ/cm²) and CNP concentrations (10–100 μM) used in this study aligned with established in vitro models investigating phototoxicity and nanoparticle-mediated protection in fibroblast cells. These parameters are consistent with prior studies modeling oxidative stress and assessing antioxidant responses in cultured fibroblasts (31, 46, 51, 52, 54). Although in vivo UVB exposure is influenced by environmental variables, the experimental settings used here provide a reliable in vitro approximation for varying levels of oxidative stress.

Prior research has demonstrated the superoxide dismutase and catalase mimetic properties of CNPs (57, 58). In the present study, the TAC assay indicated a total antioxidant capacity of 34.66 ± 1.57 nmol/mL in the control group, which increased to 118 ± 4.716 nmol/mL in the CNP-treated group. These findings are consistent with previous studies employing the xanthine/luminol/xanthine oxidase system, where CNPs were shown to inhibit ROS production in a dose-dependent manner and enhance overall antioxidant capacity (31).

Findings from the CUPRAC, DCFH-DA, flow cytometry, and TAC assays demonstrate that CNPs exert cytoprotective effects by attenuating ROS accumulation and inhibiting apoptosis in UVB-exposed L929 fibroblasts. However, given the distinct mechanisms through which UVA and UVB induce apoptosis, further investigation is needed to clarify the specific pathways by which CNPs modulate these processes and protect against UVB-induced cellular damage.

The mechanisms by which UVA and UVB induce apoptosis differ substantially. UVA primarily generates ROS through interactions with endogenous chromophores and photosensitizers, whereas UVB causes direct DNA damage, including the formation of cyclobutane pyrimidine dimers (CPDs) (59). Mitochondria, as both generators and targets of ROS, are central to this process: UV-induced ROS can trigger cytochrome c release, activate caspases, and initiate mitochondrial-mediated apoptosis (60). By neutralizing ROS at both extracellular and mitochondrial levels, CNPs appear to interrupt these pathways, offering protection against UVB-induced cellular damage in fibroblasts (61). Other studies have demonstrated that CNPs can reduce ROS generation, protect human cells from inflammation and radiation, and facilitate wound healing (62). One study reported that UVB irradiation increased ROS production in L929 fibroblasts, as evidenced by an increase in fluorescent signals compared to the control group.

However, treatment with CNPs reduced ROS levels, evidenced by a decline in fluorescence intensity relative to UVB-exposed cells (31), consistent with the present findings. Another investigation assessed the photoprotective effects of cerium oxide nanoparticles against UVA-induced aging in human skin fibroblasts (46). In that study, untreated cells and those exposed only to CNPs exhibited minimal fluorescence, whereas UVA exposure (100 mJ/cm²) significantly increased fluorescence intensity. The addition of CNPs (50 μg/mL) markedly suppressed this signal, suggesting that UVA promotes ROS generation in the epidermis and dermis, contributing to skin aging. The reduction in ROS levels observed with CNP treatment in that study parallels the antioxidant effects reported in the present work, with both studies employing similar methods for detecting reactive oxygen species.

Previous studies have also corroborated the role of CNPs in attenuating ROS-mediated apoptosis. For example, in UVA-irradiated L929 cells, CNPs demonstrated a capacity for ROS scavenging and cellular protection (45, 46). In another study using both UVB and UVA irradiation to induce apoptosis in a human melanocyte cell line, UVB was found to trigger pro-apoptotic signaling via Bax and caspase activation (20). These findings aligned with the apoptotic effects observed in the present UVB-exposed L929 cells, reinforcing the potential of CNPs as anti-apoptotic agents.

Building on these mechanistic insights, several directions can be pursued to deepen the understanding and clinical applicability of CNPs under UV exposure, particularly in light of the restricted scope of the present in vitro study and the limited range of endpoints evaluated. Incorporating assays to evaluate DNA integrity would provide more insight into the potential of CNPs for genomic protection. Comprehensive nanoparticle characterization, including stability in biological media, surface charge (zeta potential), and long-term ROS-scavenging activity, would further validate their biomedical

relevance. Growing investigations have centered on the use of antioxidant-modified combinations in ointments, a strategy known as photochemoprotection, as a preventive measure for UVB radiation-induced damages. This approach involves utilizing photoprotectors that prevent the generation of intracellular ROS in the course of or after UVB exposure (31, 51, 54). Given their dual role as UV absorbers and ROS inhibitors (63), they are potential research options for uncovering the effective or determining role they could have regarding methods of screening human skin from UVB-induced damage.

Considering the demonstrated antioxidant properties of CNPs under UV radiation, sun care products formulated with CNPs could leverage these findings to develop more effective strategies for protecting human skin against high-dose UVR exposure. Nevertheless, a recurrent limitation in related studies on ROS and antioxidants such as CNPs is the tendency to overlook their composite nature, often treating them as single molecular entities. This oversimplification may introduce ambiguity, as some antioxidants block the activity of certain species of ROS while leaving others intact (64).

In addition, the major direct effects of UVB radiation (and, to a lesser extent, UVA) are related to their absorption by DNA pyrimidine bases, which, after various excitation processes, generate cyclobutane pyrimidine dimers and comparatively fewer pyrimidine (6-4) pyrimidone photoproducts (6-4PPs) (10, 65). Accordingly, more key biomarkers of UVB radiation damage, including major CPDs and minor oxidation products like single-strand breaks (SSB) and 8-oxoguanine (8-oxoG) and breakdown lipid peroxidation products including isoprostanes and 4-hydroxynonenal, require measurement with relative assays for further accurate analytical approaches. Future studies should incorporate precise assays to measure these biomarkers in order to establish a stronger causal link between UVB exposure, CNP antioxidant activity, and cellular protection mechanisms. This will help clarify the specific components of CNPs responsible for mitigating UVB damage and define their role in modulating ROS in biological systems.

The cerium oxide nanoparticles in this study mitigated the harmful biological consequences of UVB radiation, such as oxidative stress and the induction of reactive oxygen species in L929 fibroblast cells. Moreover, the CNPs exhibited antioxidant and protective properties, demonstrating notable ROS-scavenging capacities, as evidenced by assay results. These findings contribute to the growing body of evidence on the dual functionality of CNPs as both UV absorbers and ROS scavengers, positioning them as promising candidates for future integration into ROS-targeted and UV-protective dermatological formulations. Additionally, they provide a basis for overcoming current study limitations and expanding the current literature in this area.

While this study demonstrates the potential of cerium oxide nanoparticles as photoprotective agents against UVB-induced oxidative stress in fibroblasts, it primarily assessed their overall biological influence rather than exploring the detailed cellular chemistry of ROS and CNP antioxidant properties. To address this gap, further investigation into the physicochemical interactions between CNPs and intracellular ROS pathways could enhance understanding of their mechanisms of action and optimize their application in targeted dermatological therapies. Although further studies are needed to elucidate long-term effects and mechanisms of action, these findings provide preliminary evidence for their safe use at low concentrations and their capacity to mitigate UVB-related oxidative stress. Future research should include a wider variety of skin cell types, such as keratinocytes, and investigate long-term and repeated UVB exposures to better simulate environmental and physiological conditions. Translating these in vitro findings into in vivo or clinical contexts and incorporating standard nanoparticle characterization protocols will be essential for the comprehensive preclinical evaluation of CNP-based formulations.

Acknowledgement

The study was approved by the Ethics Committees of Shiraz University of Medical Sciences (Approval Code: IR.SUMS.REC.1400.594).

References

1. D'Orazio J, Jarrett S, Amaro-Ortiz A, et al. UV radiation and the skin. Int J Mol Sci. 2013;14(6):12222-48.

2. Dupont E, Gomez J, Bilodeau D. Beyond UV radiation: a skin under challenge. Int J Cosmet Sci. 2013;35(3):224-32.
3. Gallagher RP, Lee TK. Adverse effects of ultraviolet radiation: A brief review. Prog Biophys Mol Biol. 2006;92(1):119-31.
4. Bhattacharyya A, Chattopadhyay R, Mitra S, et al. Oxidative stress: an essential factor in the pathogenesis of gastrointestinal mucosal diseases. Physiol Rev. 2014;94(2):329-54.
5. Nita M, Grzybowski A. The Role of the Reactive Oxygen Species and Oxidative Stress in the Pathomechanism of the Age-Related Ocular Diseases and Other Pathologies of the Anterior and Posterior Eye Segments in Adults. Oxid Med Cell Longev. 2016;2016:3164734.
6. Cadet J, Loft S, Olinski R, et al. Biologically relevant oxidants and terminology, classification and nomenclature of oxidatively generated damage to nucleobases and 2-deoxyribose in nucleic acids. Free Radic Res. 2012;46(4):367-81.
7. Ray PD, Huang B-W, Tsuji Y. Reactive oxygen species (ROS) homeostasis and redox regulation in cellular signaling. Cell Signal. 2012;24(5):981-90.
8. Wondrak GT, Jacobson MK, Jacobson EL. Endogenous UVA-photosensitizers: mediators of skin photodamage and novel targets for skin photoprotection. Photochem Photobiol Sci. 2006;5(2):215-37.
9. de Jager TL, Cockrell AE, Du Plessis SS. Ultraviolet Light Induced Generation of Reactive Oxygen Species. Adv Exp Med Biol. 2017;996:15-23.
10. Cadet J, Douki T, Ravanat JL. Oxidatively generated damage to cellular DNA by UVB and UVA radiation. Photochem Photobiol. 2015;91(1):140-55.
11. Baptista MS, Cadet J, Greer A, et al. Photosensitization Reactions of Biomolecules: Definition, Targets and Mechanisms. Photochem Photobiol. 2021;97(6):1456-83.
12. Jin S-G, Padron F, Pfeifer GP. UVA radiation, DNA damage, and melanoma. ACS omega. 2022;7(37):32936-48.
13. Snezhkina AV, Kudryavtseva AV, Kardymon OL, et al. ROS Generation and Antioxidant Defense Systems in Normal and Malignant Cells. Oxid Med Cell Longev. 2019;2019:6175804.
14. Kappes UP, Luo D, Potter M, et al. Short- and long-wave UV light (UVB and UVA) induce similar mutations in human skin cells. J Invest Dermatol. 2006;126(3):667-75.
15. Nichols JA, Katiyar SK. Skin photoprotection by natural polyphenols: anti-inflammatory, antioxidant and DNA repair mechanisms. Arch Dermatol Res. 2010;302(2):71-83.
16. Meinhardt M, Krebs R, Anders A, et al. Wavelength-dependent penetration depths of ultraviolet radiation in human skin. J Biomed Opt. 2008;13(4):044030.
17. Jaszewska E, Soin M, Filipek A, et al. UVA-induced ROS generation inhibition by Oenothera paradoxa defatted seeds extract and subsequent cell death in human dermal fibroblasts. J Photochem Photobiol B. 2013;126:42-6.
18. Chen L, Hu JY, Wang SQ. The role of antioxidants in photoprotection: A critical review. Journal of the American Academy of Dermatology. 2012;67(5):1013-24.
19. Aroun A, Zhong JL, Tyrrell RM, et al. Iron, oxidative stress and the example of solar ultraviolet A radiation. Photochem Photobiol Sci. 2012;11(1):118-34.
20. Bivik CA, Larsson PK, Kågedal KM, et al. UVA/B-induced apoptosis in human melanocytes involves translocation of cathepsins and Bcl-2 family members. J Invest Dermatol. 2006;126(5):1119-27.
21. Dhall A, Self W. Cerium oxide nanoparticles: a brief review of their synthesis methods and biomedical applications. Antioxidants. 2018;7(8):97.
22. Singh S, Ly A, Das S, et al. Cerium oxide nanoparticles at the nano-bio interface: Size-dependent cellular uptake. Artif Cells Nanomed Biotechnol. 2018;46(sup3):S956-S63.
23. Xu C, Qu X. Cerium oxide nanoparticle: a remarkably versatile rare earth nanomaterial for biological applications. NPG Asia Mater. 2014;6(3):e90-e.
24. Pezzini I, Marino A, Turco SD, et al. Cerium oxide nanoparticles: the regenerative redox machine in bioenergetic imbalance. Nanomedicine. 2017;12(4):403-16.
25. Xiao G-B, Meng R, Yang S, et al. Cerium oxide nanoparticle as interfacial modifier for efficient

and UV-stable perovskite solar cells. Chem Eng J. 2023;462:142047.
26. Li Y, Li P, Yu H, et al. Recent advances (2010–2015) in studies of cerium oxide nanoparticles' health effects. Environ Toxicol Pharmacol. 2016;44:25-9.
27. Pirmohamed T, Dowding JM, Singh S, et al. Nanoceria exhibit redox state-dependent catalase mimetic activity. Chem Commun. 2010;46(16):2736-8.
28. Gunawan C, Lord MS, Lovell E, et al. Oxygen-Vacancy Engineering of Cerium-Oxide Nanoparticles for Antioxidant Activity. ACS omega. 2019;4(5):9473-9.
29. Lord MS, Berret JF, Singh S, et al. Redox Active Cerium Oxide Nanoparticles: Current Status and Burning Issues. Small. 2021;17(51):e2102342.
30. Celardo I, Pedersen JZ, Traversa E, et al. Pharmacological potential of cerium oxide nanoparticles. Nanoscale. 2011;3(4):1411-20.
31. Peloi KE, Lancheros CAC, Nakamura CV, et al. Antioxidative photochemoprotector effects of cerium oxide nanoparticles on UVB irradiated fibroblast cells. Colloids Surf B Biointerfaces. 2020;191:111013.
32. Akhtar MJ, Ahamed M, Alhadlaq HA, et al. Glutathione replenishing potential of CeO_2 nanoparticles in human breast and fibrosarcoma cells. J Colloid Interface Sci. 2015;453:21-7.
33. Colon J, Hsieh N, Ferguson A, et al. Cerium oxide nanoparticles protect gastrointestinal epithelium from radiation-induced damage by reduction of reactive oxygen species and upregulation of superoxide dismutase 2. Nanomedicine. 2010;6(5):698-705.
34. Hirst SM, Karakoti A, Singh S, et al. Bio-distribution and in vivo antioxidant effects of cerium oxide nanoparticles in mice. Environ Toxicol. 2013;28(2):107-18.
35. Ray RS, Agrawal N, Sharma A, et al. Use of L-929 cell line for phototoxicity assessment. Toxicol In Vitro. 2008;22(7):1775-81.
36. Mosmann T. Rapid colorimetric assay for cellular growth and survival: application to proliferation and cytotoxicity assays. J Immunol Methods. 1983;65(1-2):55-63.
37. Berridge MV, Herst PM, Tan AS. Tetrazolium dyes as tools in cell biology: new insights into their cellular reduction. Biotechnol Annu Rev. 2005;11:127-52.
38. Ghasemi M, Turnbull T, Sebastian S, et al. The MTT Assay: Utility, Limitations, Pitfalls, and Interpretation in Bulk and Single-Cell Analysis. Int J Mol Sci. 2021;22(23).
39. Özyürek M, Güçlü K, Apak R. The main and modified CUPRAC methods of antioxidant measurement. Int J Anal Chem. 2011;30(4):652-64.
40. Eruslanov E, Kusmartsev S. Identification of ROS using oxidized DCFDA and flow-cytometry. Methods Mol Biol. 2010;594:57-72.
41. Kalyanaraman B, Darley-Usmar V, Davies KJ, et al. Measuring reactive oxygen and nitrogen species with fluorescent probes: challenges and limitations. Free Radic Biol Med. 2012;52(1):1-6.
42. Forman HJ, Augusto O, Brigelius-Flohe R, et al. Even free radicals should follow some rules: a guide to free radical research terminology and methodology. Free Radic Biol Med. 2015;78:233-5.
43. LeBel CP, Ischiropoulos H, Bondy SC. Evaluation of the probe 2',7'-dichlorofluorescin as an indicator of reactive oxygen species formation and oxidative stress. Chem Res Toxicol. 1992;5(2):227-31.
44. Khalil C, Shebaby W. UVB damage onset and progression 24 h post exposure in human-derived skin cells. Toxicology reports. 2017;4:441-9.
45. Ribeiro FM, de Oliveira MM, Singh S, et al. Ceria Nanoparticles Decrease UVA-Induced Fibroblast Death Through Cell Redox Regulation Leading to Cell Survival, Migration and Proliferation. Frontiers in Bioengineering and Biotechnology. 2020;8(1133).
46. Li Y, Hou X, Yang C, et al. Photoprotection of Cerium Oxide Nanoparticles against UVA radiation-induced Senescence of Human Skin Fibroblasts due to their Antioxidant Properties. Sci Rep. 2019;9(1):2595.
47. Kargar H, Ghasemi F, Darroudi M. Bioorganic polymer-based synthesis of cerium oxide nanoparticles and their cell viability assays. Ceram Int. 2015;41(1, Part B):1589-94.
48. Oberdörster G, Maynard A, Donaldson K, et al. Principles for characterizing the potential human health effects from exposure to nanomaterials: elements of a screening strategy. J Cell Physiol. 2005;2(1):8.

49. Park E-J, Choi J, Park Y-K, et al. Oxidative stress induced by cerium oxide nanoparticles in cultured BEAS-2B cells. Toxicology. 2008;245(1):90-100.
50. Nourmohammadi E, Khoshdel-Sarkarizi H, Nedaeinia R, et al. Evaluation of anticancer effects of cerium oxide nanoparticles on mouse fibrosarcoma cell line. J Cell Physiol. 2019;234(4):4987-96.
51. Oliveira MMd, Daré RG, Barizão ÉO, et al. Photodamage attenuating potential of Nectandra hihua against UVB-induced oxidative stress in L929 fibroblasts. J Photochem Photobiol B. 2018;181:127-33.
52. Liu W, Otkur W, Zhang Y, et al. Silibinin protects murine fibroblast L929 cells from UVB-induced apoptosis through the simultaneous inhibition of ATM-p53 pathway and autophagy. Febs j. 2013;280(18):4572-84.
53. Daré RG, Nakamura CV, Ximenes VF, et al. Tannic acid, a promising anti-photoaging agent: Evidences of its antioxidant and anti-wrinkle potentials, and its ability to prevent photodamage and MMP-1 expression in L929 fibroblasts exposed to UVB. Free Radic Biol Med. 2020;160:342-55.
54. da Silva BTA, Peloi KE, Ximenes VF, et al. 2-acetylphenothiazine protects L929 fibroblasts against UVB-induced oxidative damage. J Photochem Photobiol B. 2021;216:112130.
55. Daré RG, Kolanthai E, Neal CJ, et al. Cerium Oxide Nanoparticles Conjugated with Tannic Acid Prevent UVB-Induced Oxidative Stress in Fibroblasts: Evidence of a Promising Anti-Photodamage Agent. Antioxidants. 2023;12(1):190.
56. Lephart ED. Skin aging and oxidative stress: Equol's anti-aging effects via biochemical and molecular mechanisms. Ageing Res Rev. 2016;31:36-54.
57. Korsvik C, Patil S, Seal S, et al. Superoxide dismutase mimetic properties exhibited by vacancy engineered ceria nanoparticles. Chem Commun (Camb). 2007(10):1056-8.
58. Li Y, He X, Yin J-J, et al. Acquired Superoxide-Scavenging Ability of Ceria Nanoparticles. Int j STEM educ. 2015;54(6):1832-5.
59. Ichihashi M, Ueda M, Budiyanto A, et al. UV-induced skin damage. Toxicology. 2003;189(1):21-39.
60. Simon HU, Haj-Yehia A, Levi-Schaffer F. Role of reactive oxygen species (ROS) in apoptosis induction. Apoptosis. 2000;5(5):415-8.
61. Xue Y, Luan Q, Yang D, et al. Direct Evidence for Hydroxyl Radical Scavenging Activity of Cerium Oxide Nanoparticles. mistry C is J Phys Chem C. 2011;115(11):4433-8.
62. Chigurupati S, Mughal MR, Okun E, et al. Effects of cerium oxide nanoparticles on the growth of keratinocytes, fibroblasts and vascular endothelial cells in cutaneous wound healing. Biomaterials. 2013;34(9):2194-201.
63. Dahle JT, Arai Y. Environmental geochemistry of cerium: applications and toxicology of cerium oxide nanoparticles. Int J Public Health Res. 2015;12(2):1253-78.
64. Halliwell B. Biochemistry of oxidative stress. Biochem Soc Trans. 2007;35(Pt 5):1147-50.
65. Hudson L, Rashdan E, Bonn CA, et al. Individual and combined effects of the infrared, visible, and ultraviolet light components of solar radiation on damage biomarkers in human skin cells. Faseb j. 2020;34(3):3874-83.